



Cross-Hole Radar Scanning of Two Vertical, Permeable, Reactive-Iron Walls at the Massachusetts Military Reservation, Cape Cod, Massachusetts

Water-Resources Investigations Report 00-4145



Prepared in cooperation with the Air Force Center for Environmental Excellence

**U.S. Department of the Interior
U.S. Geological Survey**

Cover: A 250-megahertz borehole-radar antenna at the Massachusetts Military Reservation, Cape Cod, Massachusetts.

**U.S. Department of the Interior
U.S. Geological Survey**

Cross-Hole Radar Scanning of Two Vertical, Permeable, Reactive-Iron Walls at the Massachusetts Military Reservation, Cape Cod, Massachusetts

By John W. Lane Jr., Peter K. Joesten, and Jennifer G. Savoie

Water-Resources Investigation Report 00-4145

Prepared in cooperation with the Air Force Center for Environmental Excellence

**Storrs, Connecticut
2001**

U.S. DEPARTMENT OF THE INTERIOR
GALE A. NORTON, Secretary

U.S. GEOLOGICAL SURVEY
Charles G. Groat, Director

The use of firm, trade, and brand names in this report is for identification purposes only and does not constitute endorsement by the U.S. Geological Survey.

For additional information write to:

Branch Chief
U.S. Geological Survey
11 Sherman Place, U-5015
Storrs, CT 06269
<http://water.usgs.gov/ogw/bgas>

Copies of this report can be purchased from:

U.S. Geological Survey
Branch of Information Services
Box 25286, Federal Center
Denver, CO 80225
<http://www.usgs.gov>

CONTENTS

Abstract.....	1
Introduction.....	2
Numerical and Physical Modeling of Vertical, Permeable, Zero-Valent, Reactive-Iron Walls.....	4
Numerical Modeling.....	4
Physical Modeling.....	8
Collection, Processing, and Analysis of Geophysical Data.....	11
Electromagnetic Induction.....	11
Borehole Deviation.....	13
Cross-Hole Radar Scanning.....	13
Summary.....	16
References Cited.....	17

FIGURES

1. Map showing location of the study area and the CS-10 plume, Massachusetts Military Reservation, Cape Cod, Mass.....	2
2. Conceptual diagram of contaminated ground water passing through a zero-valent reactive-iron wall.....	3
3. Conceptual diagram showing the effects of iron distribution and discontinuities on the transmission of radar waves.....	4
4. Diagram of the two-dimensional finite-difference time-domain numerical model used for this study.....	5
5. Graph showing waveform characteristics of the 250-megahertz Ricker wavelet used for the numerical modeling and a 250-megahertz transmitted radar wave from the field data.....	5
6. Diagram of the two-dimensional finite-difference time-domain numerical model geometry used to determine the effects of wall edges on radar transmission characteristics.....	6
7. Diagram of the two-dimensional finite-difference time-domain numerical model geometry used to determine the effects of wall discontinuities (holes) on radar transmission characteristics.....	6
8. Plot of two-dimensional finite-difference time-domain numerical model radar-pulse amplitude results normalized to background amplitudes.....	7
9. Plot of two-dimensional finite-difference time-domain numerical radar-waveform results plotted as a function of time.....	7
10. Graph of two-dimensional finite-difference time-domain numerical model results showing normalized maximum peak-to-peak amplitude plotted against hole aperture.....	8
11. Photograph of the physical model assembly with the perfect-conductor analog extending half of the length of the tank.....	9
12. Conceptual diagram of the physical model assembly consisting of a tank filled with saturated sand and a perfect-conductor analog extending the length of the tank.....	9

13. Conceptual diagram of the physical model assembly with a perfect-conductor analog extending half of the length of the tank.....	9
14. Conceptual diagram of the physical model assembly containing a perfect-conductor analog with holes of apertures 0.36 and 2.00 wavelengths.....	9
15. Plot of a waveform transmitted through the background physical model and a waveform transmitted through the perfect-conductor analog.....	10
16. Plot of radar data from the half-wall physical model overlain with results from the half-wall numerical model.....	11
17. Plot of normalized peak-to-peak amplitudes for waves transmitted in the physical model through the perfect-conductor analog for holes of 0.36 and 2.00 wavelengths	11
18. Map view of the study area showing observation boreholes and transmission raypaths, Massachusetts Military Reservation, Cape Cod, Mass.....	12
19. Graph of borehole electromagnetic logging of boreholes north of the A-wall after the A-wall installation, Massachusetts Military Reservation, Cape Cod, Mass.....	12
20. Plot of pre-injection direct-wave amplitudes across the B-wall, Massachusetts Military Reservation, Cape Cod, Mass.....	13
21. Plot of post-injection direct-wave amplitudes across the A-wall, Massachusetts Military Reservation, Cape Cod, Mass.....	14
22. Plot of post-injection direct-wave amplitudes across the B-wall, Massachusetts Military Reservation, Cape Cod, Mass.....	14
23. Map view of the study area showing observation boreholes and transmission raypaths lost due to damaged boreholes, Massachusetts Military Reservation, Cape Cod, Mass.....	14
24. Plot of normalized model-wall amplitudes for a 3.10-meter wall and the normalized field-data amplitudes from the common-depth radar survey between boreholes RW-20 and RW-13, Massachusetts Military Reservation, Cape Cod, Mass.....	15
25. Plot of post-injection direct-wave amplitudes across the A-wall showing normalized amplitudes of less than 0.43, Massachusetts Military Reservation, Cape Cod, Mass.....	15
26. Plot of post-injection direct-wave amplitudes across the B-wall showing normalized amplitudes of less than 0.43, Massachusetts Military Reservation, Cape Cod, Mass.....	15

CONVERSION FACTORS AND ABBREVIATIONS

Multiply	By	To obtain
centimeter (cm)	0.3937	inch (in)
meter (m)	3.281	foot (ft)

Other abbreviations used in this report:

mV, microvolt
 MHz, megahertz
 S/m, siemens per meter

Cross-Hole Radar Scanning of Two Vertical, Permeable, Reactive-Iron Walls at the Massachusetts Military Reservation, Cape Cod, Massachusetts

By John W. Lane Jr., Peter K. Joesten, and Jennifer G. Savoie

ABSTRACT

A pilot-scale study was conducted by the U.S. Army National Guard (USANG) at the Massachusetts Military Reservation (MMR) on Cape Cod, Massachusetts, to assess the use of a hydraulic-fracturing method to create vertical, permeable walls of zero-valent iron to passively remediate ground water contaminated with chlorinated solvents. The study was conducted near the source area of the Chemical Spill-10 (CS-10) plume, a plume containing chlorinated solvents that underlies the MMR. Ground-water contamination near the source area extends from about 24 m (meters) to 35 m below land surface. The USANG designed two reactive-iron walls to be 12 m long and positioned 24 to 37 m below land surface to intersect and remediate part of the CS-10 plume.

Because iron, as an electrical conductor, absorbs electromagnetic energy, the U.S. Geological Survey used a cross-hole common-depth, radar scanning method to assess the continuity and to estimate the lateral and vertical extent of the two reactive-iron walls. The cross-hole radar surveys were conducted in boreholes on opposite sides of the iron injection zones using electric-dipole antennas with dominant center frequencies of 100 and 250 MHz. Significant decreases in the radar-pulse amplitudes observed in scans that traversed the injection zones were interpreted by

comparing field data to results of two-dimensional finite-difference time-domain numerical models and laboratory-scale physical models.

The numerical and physical models simulate a wall of perfectly conducting material embedded in saturated sand. Results from the numerical and physical models show that the amplitude of the radar pulse transmitted across the edge of a conductive wall is about 43 percent of the amplitude of a radar pulse transmitted across background material. The amplitude of a radar pulse transmitted through a hole in a conductive wall increases as the aperture of the hole increases. The modeling results indicate that holes with an aperture of less than 40 percent of the dominant wavelength of the radar pulse are not likely to be detected.

Based on the results of the numerical and physical modeling, the decreases in radar-pulse amplitudes observed in scans traversing the injection zones are interpreted as electrically conductive zones that outline the distribution of iron. The area interpreted as iron in the northern A-wall contains two zones -- an upper zone about 10 m wide, extending from about 25 to 31 m below land surface, and a lower zone about 8 m wide, extending from 31.5 to 34.5 m below land surface. The area interpreted as iron in the southern B-wall is about 9 m wide, extending from about 27 to 34.5 m below land surface. No discrete holes were interpreted in either the A- or B-wall zones.

The interpretation of the field data suggests that (1) the hydraulic-fracturing method introduced iron into the subsurface, but not in the dimensions originally proposed; (2) the iron within the treatment zones is distributed in a generally continuous manner; and (3) excluding the discontinuity in the A-wall, holes within the iron treatment zone, if any, exist at scales smaller than about 10 cm, the resolution limit of the radar antennas and acquisition geometry used for this study. The cross-hole radar method appears to have been an effective method for delineating the distribution of iron in the two walls; however, the veracity of the results cannot be ascertained without excavation or drilling into the treatment zone.

INTRODUCTION

Ground water beneath and downgradient from the Massachusetts Military Reservation (MMR), on Cape Cod, Massachusetts, has been affected by contaminants used during past decades of military operations (Savoie and LeBlanc, 1998). Chlorinated solvents that have entered the ground-water system are moving away from the MMR in the underlying sand-and-gravel aquifer toward streams, ponds, and coastal bays. Chemical Spill-10 (CS-10) is a chlorinated-solvent plume that emanates from a site used from 1960 to 1973 by the U.S. Air Force to house and maintain the Boeing Michigan Aerospace Research Center (BOMARC) ground-to-air missiles and launcher systems (fig. 1) (ABB Environmental Services, Inc., 1993). From 1978 to the present, the site has been used by the U.S. Army National Guard to store and maintain armored and military vehicles. Primary sources of contamination were caused by chemical spills and from the disposal of

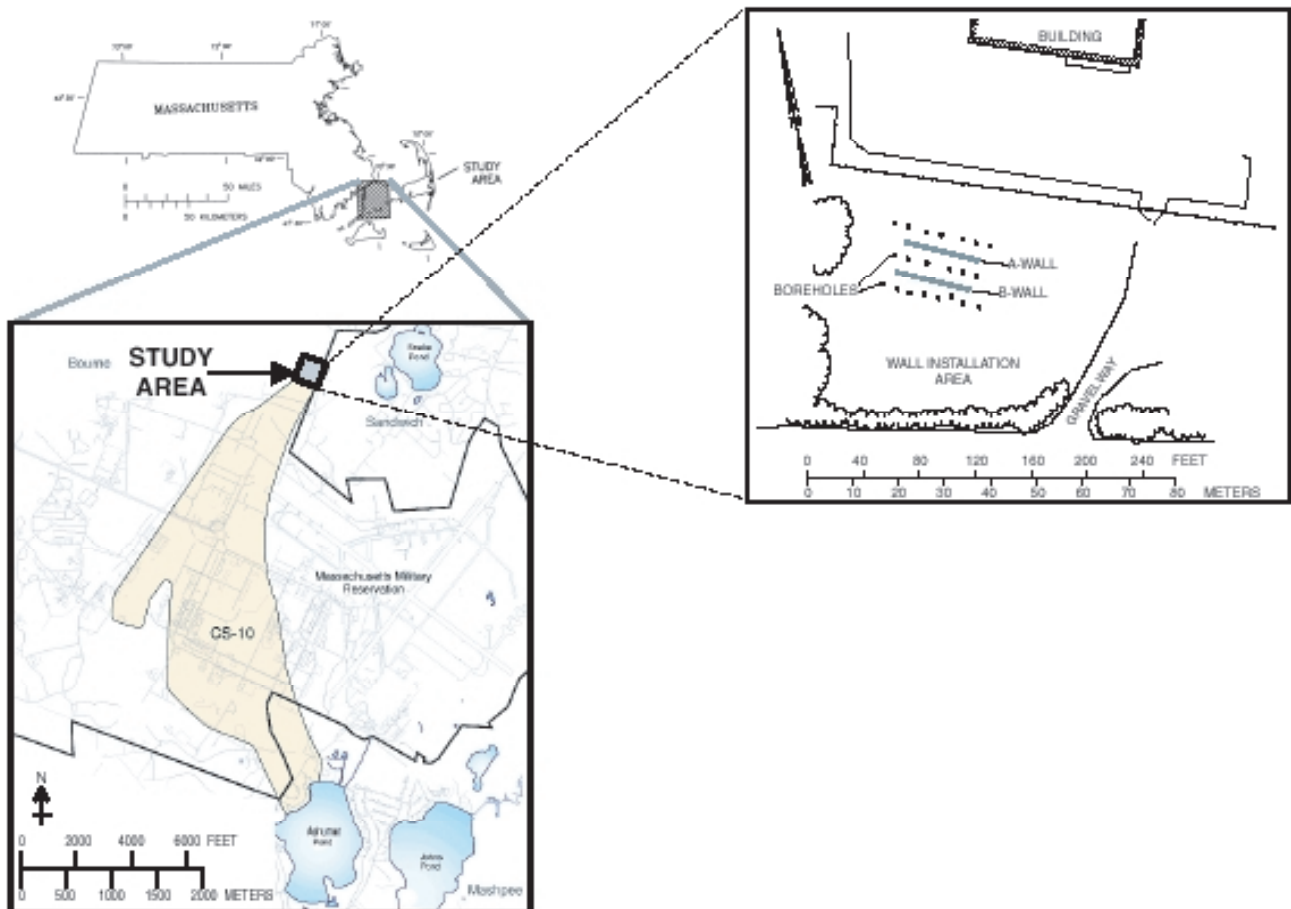


Figure 1. Location of the study area and the CS-10 plume, Massachusetts Military Reservation, Cape Cod, Mass.

chemical wastes in leaching wells and oil interceptors (ABB Environmental Services, Inc., 1993). The contaminants in the ground water of greatest concern include trichloroethene (TCE) and tetrachloroethene (PCE) (ABB Environmental Services, Inc., 1993).

To prevent continued spread of these chemicals from the source area, the MMR Installation Restoration Program contracted with the University of Waterloo to design and manage the installation of a pilot-scale permeable zero-valent iron remediation system in the path of the plume downgradient from the source area. Zero-valent iron has been used to remediate ground water contaminated with chlorinated solvents at several sites in North America and Europe (Gillham and O'Hannesin, 1994). Permeable walls of zero-valent iron can provide a relatively inexpensive alternative to pump-and-treat technology. The method does not require the withdrawal of ground water, thus minimizing changes to ambient water levels and natural ground-water flow. At many of these sites, a funnel-and-gate system has been implemented (Starr and Cherry, 1994; Smyth and others, 1996). In this system, an impermeable barrier, which often consists of sheet piling, channels ground water towards a gate, which is filled with zero-valent granular iron filings. As contaminated ground water moves through the treatment zone, chlorinated solvents are reductively dechlorinated to less harmful chemicals (Gillham and O'Hannesin, 1994).

The CS-10 plume at the former BOMARC site is 24 to 37 m below land surface. Because these depths exceed the practical limit for the funnel-and-gate method, an alternative installation method was required to use zero-valent iron to remediate the CS-10 plume. The installation method selected for the CS-10 plume was hydraulic fracturing (Hubble and Gillham, 1997, 1999; Hubble and others, 1997). The hydraulic fracturing uses a proprietary injection technology to install permeable zero-valent reactive-iron walls in unconsolidated sediments (Grant Hocking and S.L. Wells, Golder Sierra LLC, written commun., 1997).

In 1998, a pilot-scale test of the hydraulic-fracturing installation method was conducted near the source area of the CS-10 plume. Two parallel, vertical iron walls (fig. 1) were emplaced to intersect contaminated ground water from 24 to 37 m below land surface. The pilot-scale test was designed to demonstrate the application of the in-place remediation technology and the vertical hydraulic-fracturing method

of installation. The CS-10 plume posed a particular challenge for vertical wall installation because the site, on a glacial outwash plain composed of interbedded sand and gravel, has a 24-m-thick unsaturated zone. The depth of the installation prevented physical inspection of the walls; therefore a remote-sensing method was required to determine the boundaries and continuity of the walls.

The U.S. Geological Survey (USGS), in cooperation with the U.S. Air Force Center for Environmental Excellence, conducted a study using cross-hole common-depth (CD) radar scanning as a remote-sensing method to determine the lateral and vertical extent of the iron walls and to determine whether large holes were present in the iron walls that could allow contaminated ground water to pass untreated through the remediation zone (fig. 2). The cross-hole radar method was chosen because a radar pulse can be significantly absorbed by accumulations of iron particles between a radar transmitter and receiver (fig. 3). To constrain the estimates of wall boundaries and continuity, the effect of wall edges and holes on the cross-hole radar data was predicted through numerical and physical modeling. In this report, the results of numerical and physical modeling are presented, and the cross-hole radar field data are interpreted to estimate the vertical and lateral distribution and continuity of two vertical, permeable, zero-valent iron walls installed near the source area of the CS-10 plume at the MMR.

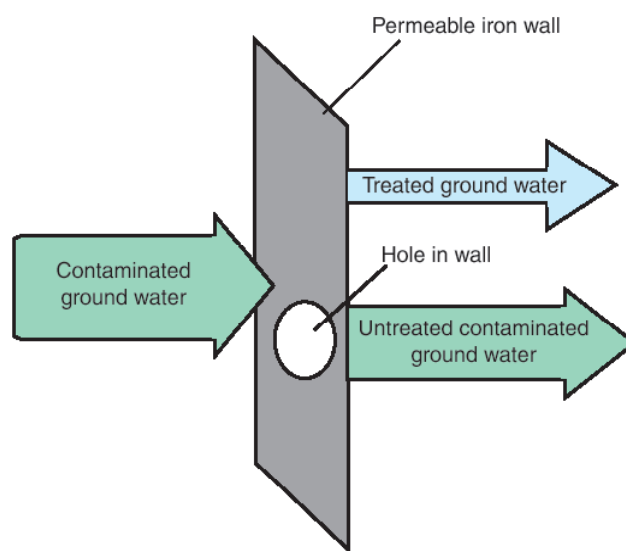


Figure 2. Conceptual diagram of contaminated ground water passing through a zero-valent reactive-iron wall.

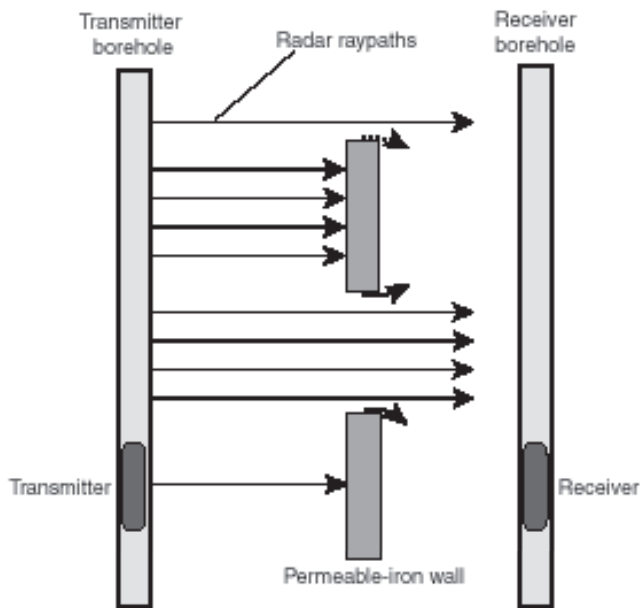


Figure 3. Conceptual diagram showing the effects of iron distribution and discontinuities on the transmission of radar waves.

The authors thank the U.S. Air Force Center for Environmental Excellence at the Massachusetts Military Reservation, Cape Cod, Mass., Edward L. Pesce, Rose Forbes, Michael Minior, and the U.S. Army National Guard for their support. The authors gratefully acknowledge David Hubble of the University of Waterloo for his assistance, Lei Xiao and Dr. Lanbo Liu of the University of Connecticut for the use of the finite-difference numerical model, and Dr. Roelof Versteeg and Justin Kuczynski of the Aldridge Geophysical Imaging Laboratory at Columbia University for their assistance with the physical modeling.

NUMERICAL AND PHYSICAL MODELING OF VERTICAL, PERMEABLE, ZERO-VALENT, REACTIVE-IRON WALLS

Conventional radar tomography methods use the travel-time or amplitude of the directly transmitted radar pulse acquired from many different transmitter-receiver pairs to generate a model of subsurface properties, such as velocity or attenuation, that can be interpreted as images. For this study,

the wall-construction materials and vertical-emplacement geometry imposed constraints on the use of conventional tomographic-imaging methods. Because the iron used in the construction of the walls absorbs radar waves, large regions of the iron injection zones were expected to act as perfect conductors that would completely block directly transmitted radar pulses. Perfect conductors are opaque to the radar, and as a result, many measurements needed for tomographic imaging are unavailable, which in turn degrades the quality, resolution, and uniqueness of tomograms produced from the cross-hole radar data.

Instead of using conventional tomographic-image reconstruction methods, radar field data were analyzed by using the results of numerical and physical models developed to predict the effects of wall edges and holes on CD cross-hole radar measurements. The use of the perfect conductor conceptual model reduces the imaging problem to the identification of (1) conductor edges and (2) holes in the conductor. This simplifies cross-hole radar data acquisition by limiting measurements to horizontal scans acquired from radar transmitters and receivers located at common depths.

Numerical Modeling

For this study, the effect of wall edges and holes on CD cross-hole radar amplitudes was determined using a two-dimensional finite-difference time-domain (2D FDTD) model developed by Xiao and others (1998). The finite-difference grid for the numerical models contained 5- by 5-cm cells, and the model domain extended 12.8 m (256 cells) in both the horizontal and vertical directions (fig. 4). The outer 2.5 m (50 cells) of the model domain is a super-absorbing boundary, designed to minimize spurious model-boundary reflection effects (Xiao and others, 1998). The electromagnetic properties of simulated materials in the model domain were chosen to be consistent with field measurements at the site. The model simulated a saturated sand with a relative dielectric permittivity (ϵ_r) of 25, an electrical conductivity (σ) of 0.01 S/m, and a relative magnetic permeability (μ_r) of 1.00 (Lane and others, 1999). Because the electrical conductivity of iron is so high (1×10^7 S/m) (Carmichael, 1989), the model wall was approximated as a near-perfect conductor, with a thickness of 10 cm.

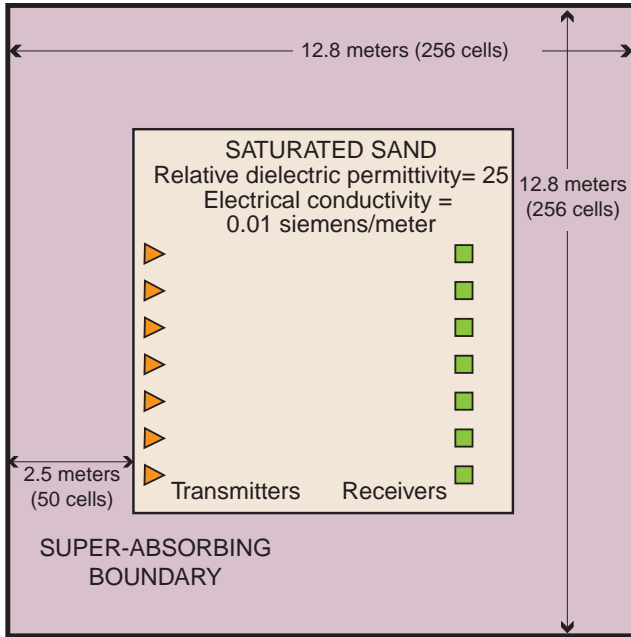


Figure 4. The two-dimensional finite-difference time-domain numerical model used for this study. [The model extends 12.8 meters (256 cells) in the vertical direction and 12.8 meters (256 cells) in the horizontal direction. There is a 2.5-meter (50 cell) super-absorbing boundary on the model to minimize edge effects (Xiao and others, 1998).]

The cross-hole radar pulse was simulated using a Ricker wavelet (Ricker, 1953) with a center frequency of 250-MHz. The pulse had a wavelength in saturated sand of about 24 cm. The frequency of the simulated radar pulse was chosen to approximate the center frequency of the borehole radar antennas used for the field study. The Ricker wavelet was selected for the numerical modeling because the shape of this wavelet approximates the waveform produced by the radar antennas used for the field study (fig. 5). Time-domain waveforms produced by the numerical models were sampled at 5,270 MHz using 1,024 samples per waveform. This sampling rate was selected to ensure that the frequency components within the radar-pulse frequency band were properly recorded.

A model that contained a 10-cm thick vertical wall extending from the center of the model domain to the model boundary (fig. 6) was used to determine the effect of wall edges on the directly transmitted cross-hole radar pulse. The model simulated a CD radar scan by stepping the transmitter and receiver locations in 10-cm intervals along the

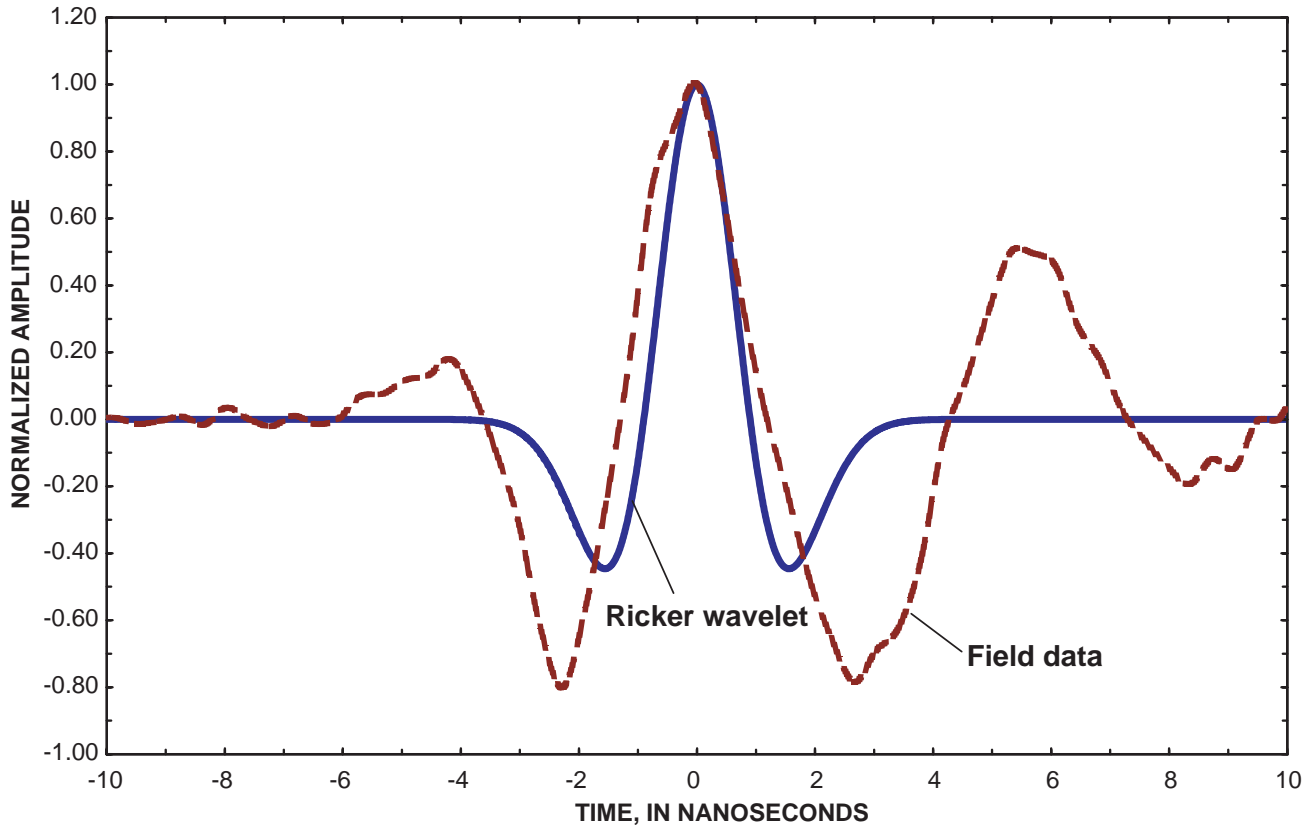


Figure 5. Waveform characteristics of the 250-megahertz Ricker wavelet used for the numerical modeling and a 250-megahertz transmitted radar wave from the field data.

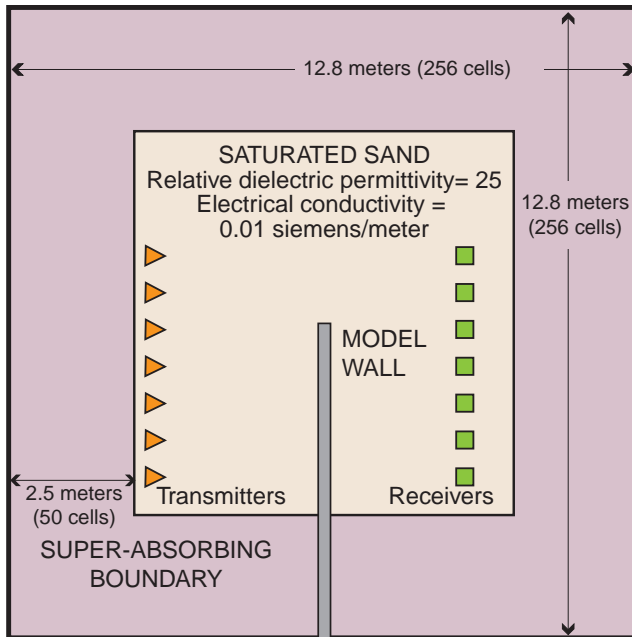


Figure 6. The two-dimensional finite-difference time-domain numerical model geometry used to determine the effects of wall edges on radar transmission characteristics.

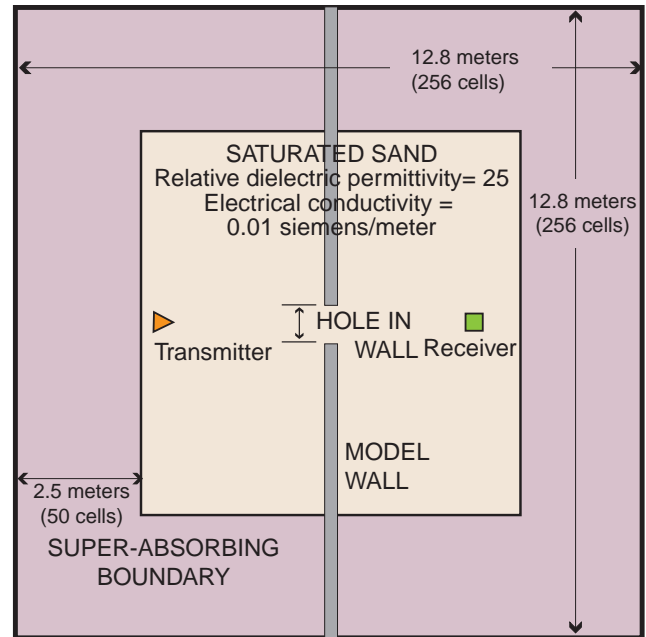


Figure 7. The two-dimensional finite-difference time-domain numerical model geometry used to determine the effects of wall discontinuities (holes) on radar transmission characteristics.

model boundary parallel to the simulated wall. The horizontal separation between the radar transmitter and receiver ranged from 5.00 to 7.25 m to simulate the distances between boreholes at the field site.

To determine the effect of discontinuities on cross-hole radar measurements, the vertical wall was extended across the entire model except for an opening centered at the midpoint of the wall (fig. 7). The separation of the transmitting and receiving antennas was fixed at 6.30 m, centered about the hole. The size of the hole ranged from 0 to 40 cm, in 5-cm increments. Relative to the transmitted radar pulse, the dimensions of the hole ranged from 0 to almost 1.7 times the wavelength of the transmitted pulse.

For each model, the 2D FDTD code produced a number of radar waveforms equal to the number of transmitter-receiver locations in the model. To determine the effect of wall edges and discontinuities on the cross-hole radar measurements, the amplitudes of the horizontal scans were measured and plotted relative to the appropriate independent variable, such as depth or hole-size.

Radar-pulse amplitudes from the edge models are shown in figure 8. The modeled pulse amplitudes were normalized to 1.0 based on an average background pulse amplitude obtained from a model without a wall. For the range of horizontal transmitter-receiver separations in this study, the simulated radar-pulse amplitude decreased to 0.43 of the normalized background wave amplitude when the modeled CD scan was at the edge of the wall.

Radar-pulse waveforms from the hole models are shown in figure 9. Qualitatively, the amplitude of the transmitted radar pulse increases as the aperture of the hole increases, approaching the amplitude of the background pulse as the size of the hole approaches the wavelength of the dominant frequency of the radar pulse. The maximum normalized amplitude of the transmitted pulse is plotted against the aperture of the hole (fig. 10). Differences in pulse amplitude are minor for holes smaller than 0.40 wavelengths (about 10 cm for a 250-MHz transmitted pulse). These results indicate that holes smaller than about 40 percent of the radar-pulse wavelength are not likely to be detected.

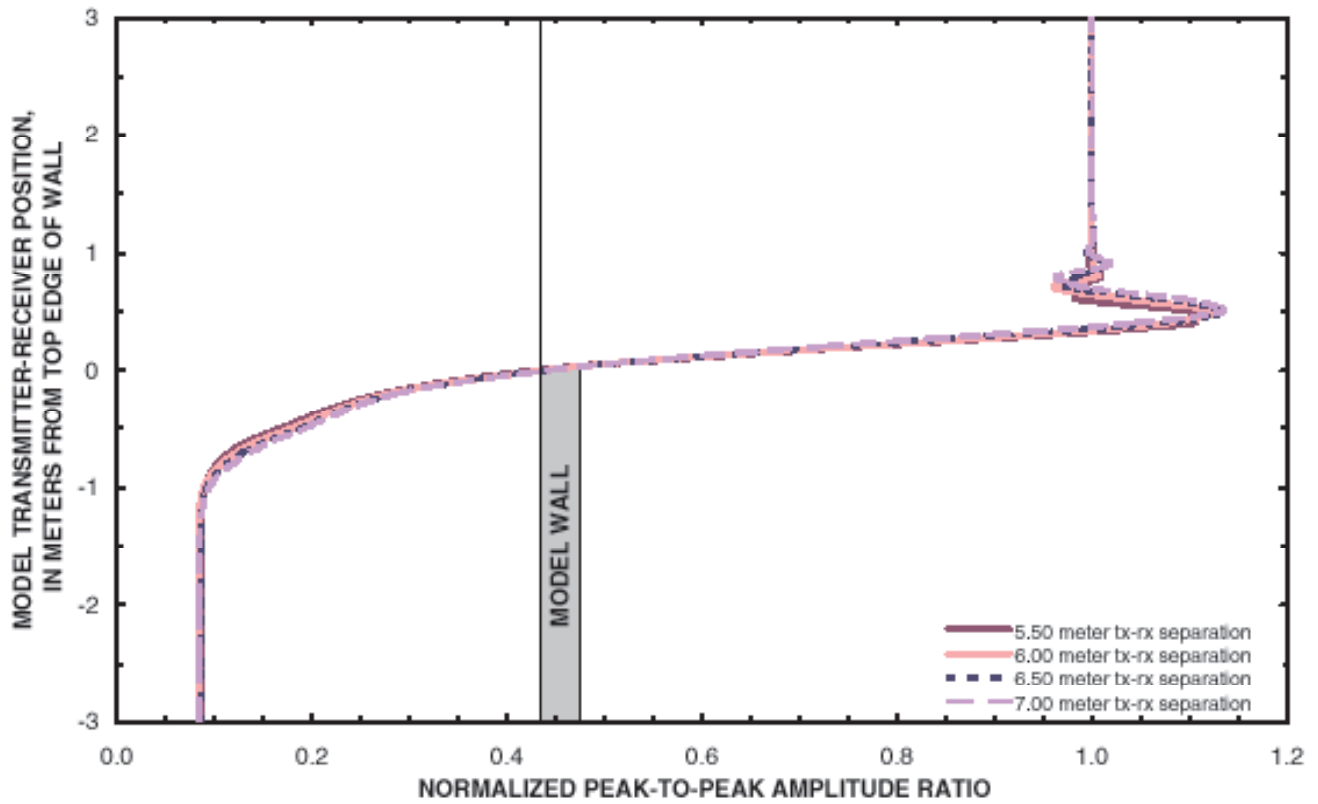


Figure 8. Two-dimensional finite-difference time-domain numerical model radar-pulse amplitude results normalized to background amplitudes. [For transmitter (tx) - receiver (rx) separations ranging from 5.50 to 7.00 meters and plotted from 3.0 meters above top edge to 3.0 meters below top edge of the wall.]

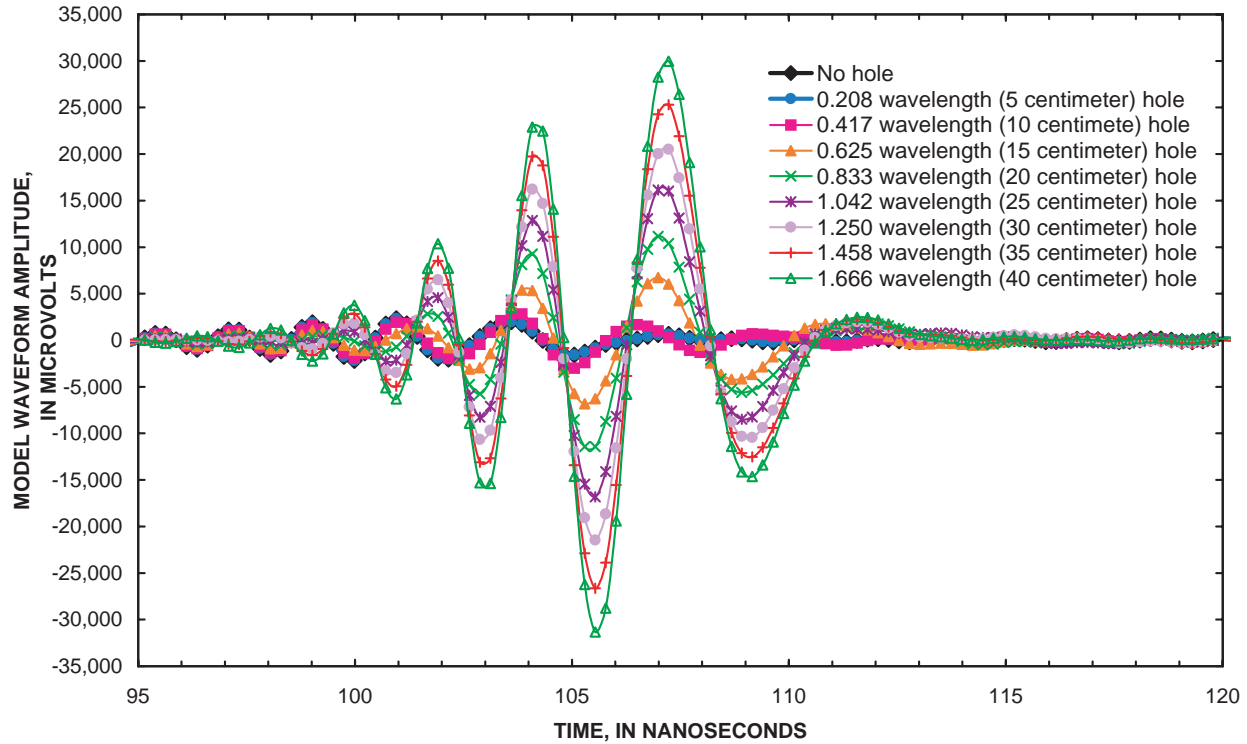


Figure 9. Two-dimensional finite-difference time-domain numerical model radar-waveform results plotted as a function of time. [Transmitter-receiver separation is 6.30 meters. Antennas are centered about holes ranging in aperture from 0 to 1.666 wavelengths (0 to 40 cm).]

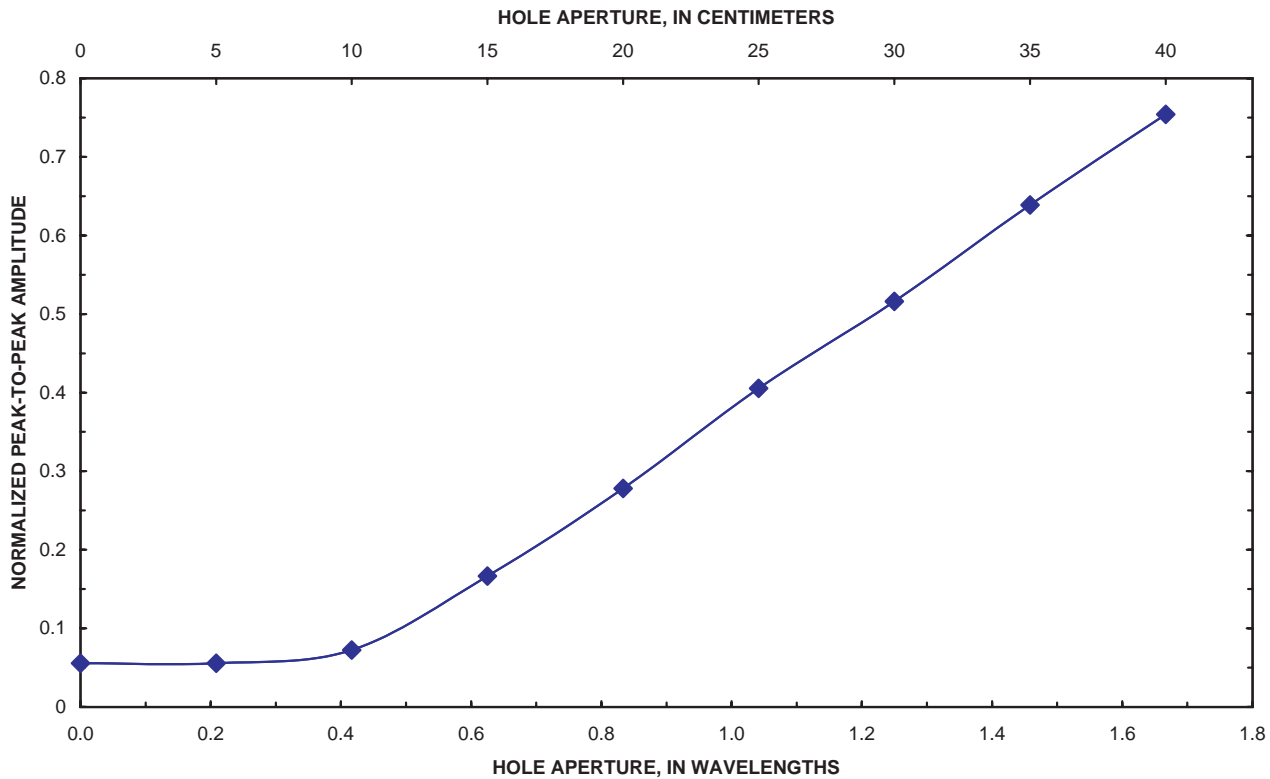


Figure 10. Two-dimensional finite-difference time-domain numerical model results showing normalized maximum peak-to-peak amplitude plotted against hole aperture.

Physical Modeling

Although the numerical modeling results indicate that wall edges and discontinuities will have predictable and measurable changes in the amplitude of a transmitted radar pulse during cross-hole radar measurements, it is appropriate to question the validity of the results. For example, are the pulse-amplitude characteristics predicted by the numerical models consistent with real data? Can the numerical-modeling results be used reliably as a template to interpret field data? Because the field problem is innovative and the borehole-radar method is relatively new, data from similar problems were not found. Therefore, the numerical-modeling results were compared to radar data obtained from laboratory-scale physical models that attempted to simulate the geometry and dimensions of the numerical models relative to the wavelength of the transmitted pulse. Scaled physical modeling was conducted at the Aldridge Geophysical Imaging Laboratory at Columbia University.

The laboratory-scale physical model was constructed from an ordinary aquarium with interior

dimensions of 119.4 by 43.3 by 75.0 cm. The aquarium was filled with sand saturated with water. A perfect conductor was simulated by wrapping 20 layers of aluminum foil around a cardboard template (fig. 11). Two Malå GeoScience RAMAC antennas with approximate center frequencies of 900 MHz were used as the transmitter and receiver (fig. 12). Radar-transmission data were acquired by moving the transmitting and receiving antennas, positioned on opposite sides of the tank 43.3 cm apart, along the 119.4-cm-long horizontal axis of the tank in 1-cm increments. Radar traces were recorded at 55,828 MHz using 1,024 samples per trace. This sampling rate was selected to ensure that frequency components within the radar-pulse frequency band were properly recorded.

Another model was constructed with the aluminum foil template extending across one-half of the tank (fig. 13). This model was designed as a physical analog to the field-scale problem simulated by the wall-edge numerical models. Two additional models were constructed with the aluminum foil template extending across the entire tank. In these models, a hole was cut into the center of each sheet

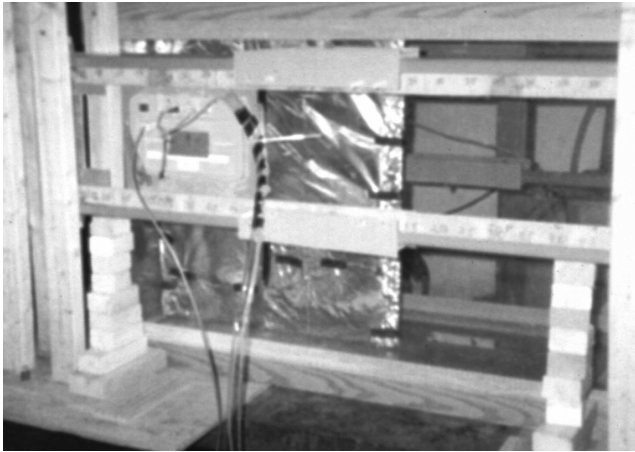


Figure 11. Physical model assembly with the perfect-conductor analog extending half of the length of the tank.

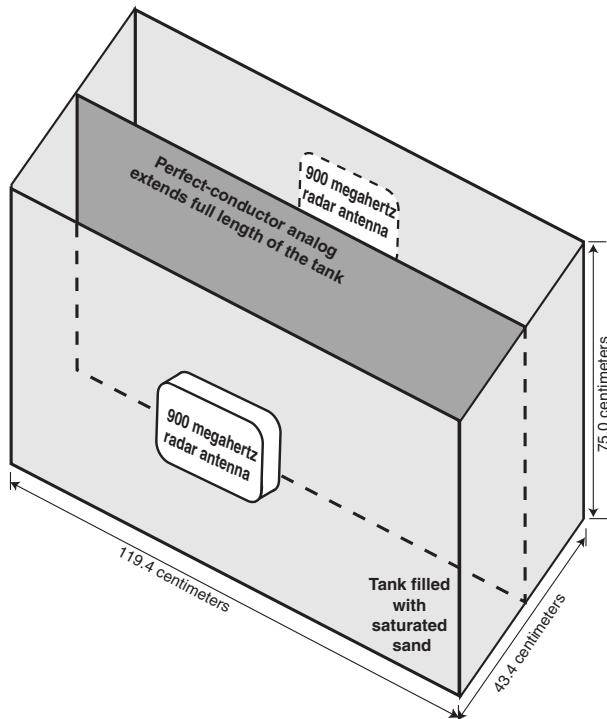


Figure 12. Conceptual diagram of the physical model assembly consisting of a tank filled with saturated sand and a perfect-conductor analog extending the length of the tank.

(fig. 14). The sizes of the holes were 2 cm and 11 cm, corresponding to about 0.36 and 2.00 wavelengths, respectively. These models were designed as physical analogs to the field-scale problem simulated by the hole-in-wall numerical models.

To determine background transmitted-pulse amplitudes and wavelengths, measurements were made across the tank containing only saturated sand. Measurements also were made with a continuous aluminum foil template placed in the tank to verify the assumption that the aluminum foil would simulate a

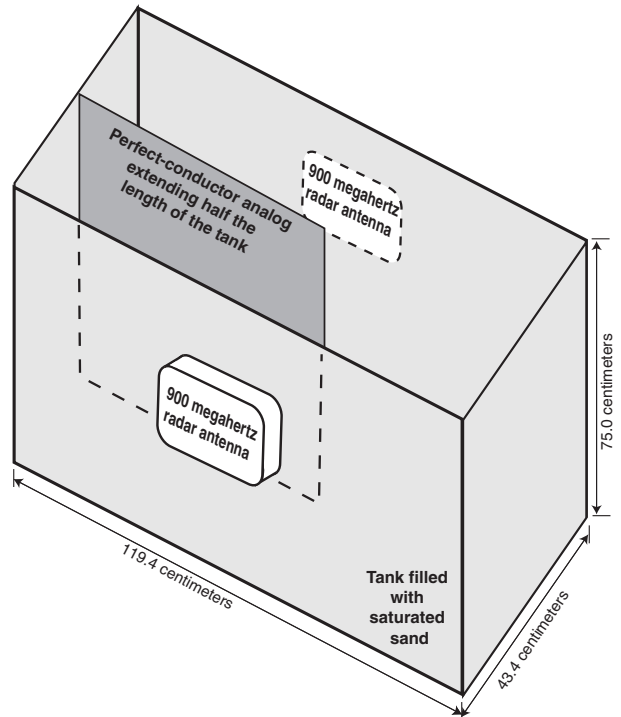


Figure 13. Conceptual diagram of the physical model assembly with a perfect-conductor analog extending half of the length of the tank.

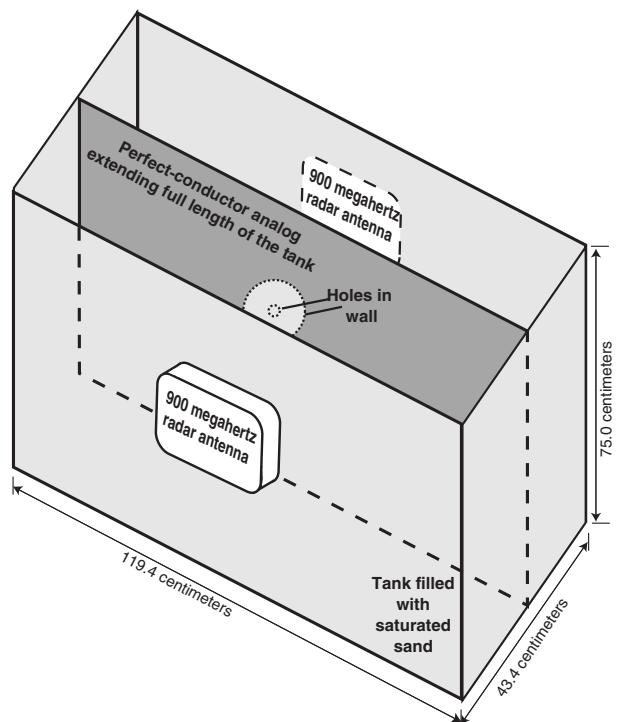


Figure 14. Conceptual diagram of the physical model assembly containing a perfect-conductor analog with holes with apertures of 0.36 and 2.00 wavelengths (2 and 11 centimeters).

perfect conductor and prevent the penetration of the radar pulse across the tank. A background radar trace is shown in figure 15. The average wavelength of the transmitted pulse in the saturated sand of the laboratory tank was 5.5 cm, with an average amplitude of about 40,000 mV. A cross-tank radar trace recorded after a continuous aluminum foil template was placed in the tank is also shown in figure 15. The amplitude of this pulse is about 0.1 percent of the background pulse amplitude, indicating that the aluminum sheet is useful for modeling a perfect conductor.

The wavelength of the pulse in saturated sand produced by the 250-MHz borehole antennas used for the field study was 24 cm, about 4 times longer than the wavelength of the antennas used for the physical model. Relative to the transmitted pulse wavelength, the laboratory tank dimensions correlate with those numerical models that simulate a borehole separation of about 2 m. The 2-cm and 11-cm holes in the aluminum sheets correlate with numerical models that contain 8.7-cm and 48-cm-diameter holes, respectively.

Maximum cross-tank radar pulse amplitudes from the half-wall physical model are shown plotted against antenna positioning in figure 16. Pulse amplitudes from the physical model have been normalized to the average background pulse amplitude. The physical-model data are shown juxtaposed to the

numerical-model results for the case of a borehole separation of 5 m. The transmitted pulse amplitude is observed to decrease as the antenna positions approach the edge of the aluminum model wall. The transmitted pulse amplitude is expected to decrease in areas where the wall is present and increase with distance away from the wall. The edge of the aluminum sheets correlates with the position of the scan where the normalized transmitted pulse amplitude decreases to about 0.41 (fig. 16). The characteristics of transmitted pulse amplitude with respect to conductor edges observed in the physical model correlates closely with the results of the 2D FDTD model, where the position of the wall edge corresponds to a decrease in normalized radar-pulse amplitude of about 0.43.

Cross-tank radar-wave amplitudes from the models constructed with a hole cut in a continuous aluminum foil template are shown in figure 17. Radar-wave amplitudes, normalized to the average background pulse amplitude, are plotted against antenna position. The transmitted pulse amplitude is observed to increase as the antenna position approaches the position of the hole in the aluminum sheets. The changes in transmitted pulse amplitude and the relative magnitude of the amplitude changes with respect to the size and location of the holes observed in the physical model data correlate closely

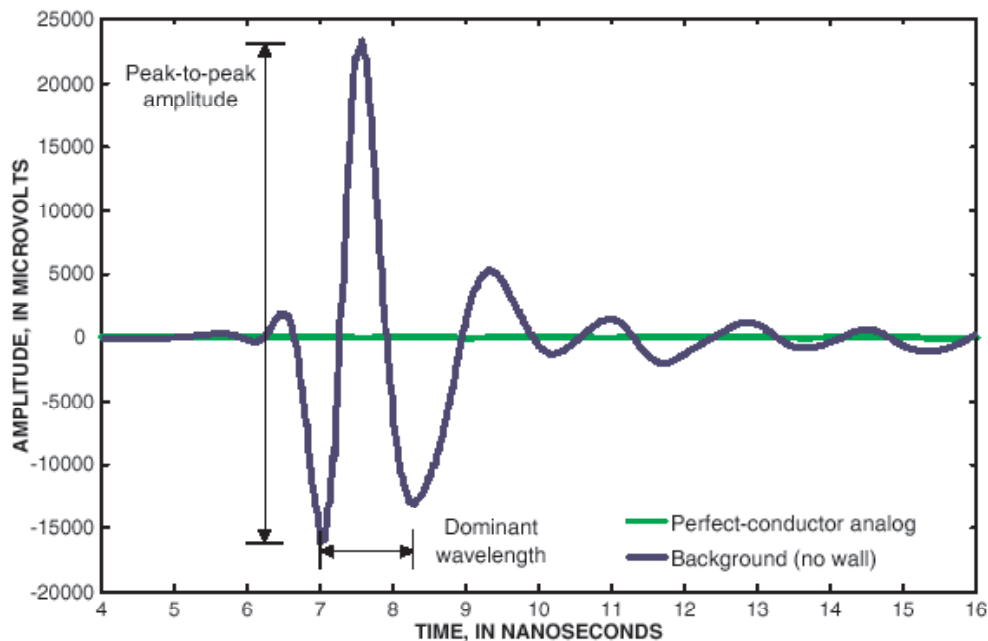


Figure 15. A waveform transmitted through the background physical model (no wall) and a waveform transmitted through the perfect-conductor analog. [The maximum amplitude of the waveform transmitted through the perfect-conductor analog is about 0.1 percent of the maximum amplitude of the waveform transmitted through the background physical model.]

COLLECTION, PROCESSING, AND ANALYSIS OF GEOPHYSICAL DATA

In this study, conventional geophysical logging and cross-hole radar scanning were conducted at the field site before and after iron injection. The conventional logs included electromagnetic (EM)-induction and borehole deviation. The conventional geophysical logging was conducted to (1) identify lithologic or water-quality changes that could affect the planning or implementation of the iron injection, (2) determine the geometry of the boreholes, and (3) provide a record of conditions near the observation boreholes to determine if any effects of the hydraulic-fracturing process could be measured using EM induction logging.

A total of 26 observation boreholes were installed at the field site. Of these, 20 were used for the study (fig. 18). Most boreholes were 7.62-cm diameter PVC cased boreholes drilled to depth of about 46 m. Five boreholes (RW-04, RW-05, RW-11, RW-13, and RW-21) were “Slope-Indicator” boreholes that utilize a specialized 6.78-cm PVC casing. The Slope-Indicator wells were used by the University of Waterloo to determine deviation from vertical.

Five boreholes (RW-03, RW-04, RW-05, RW-11, and RW-12) were damaged during the wall installation and could not be used for additional radar logging. Three new boreholes (RW-03A, RW-04A, and RW-11A) were installed to replace the damaged boreholes. Borehole RW-21 deviated through the expected path of the wall, thus it could not be used to interpret accurately the wall location using cross-hole methods.

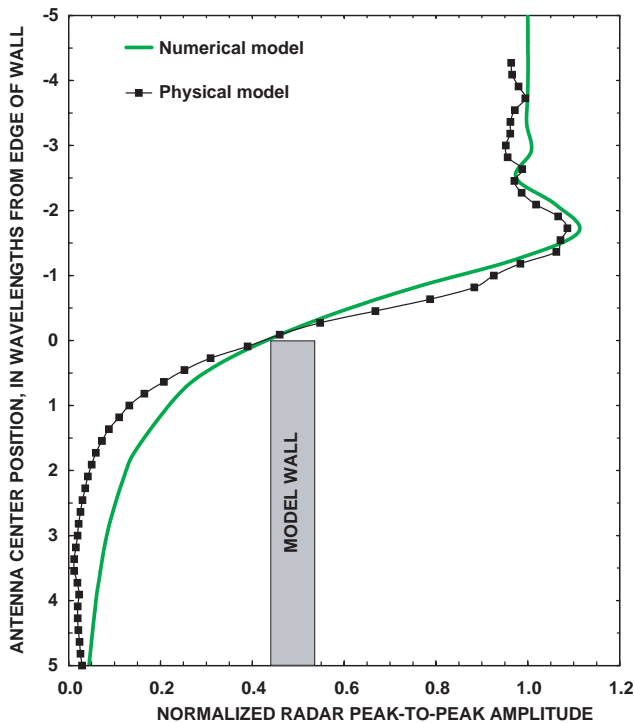


Figure 16. Radar data from the half-wall physical model overlain with results from the half-wall numerical model [for an antenna separation of 5.00 meters].

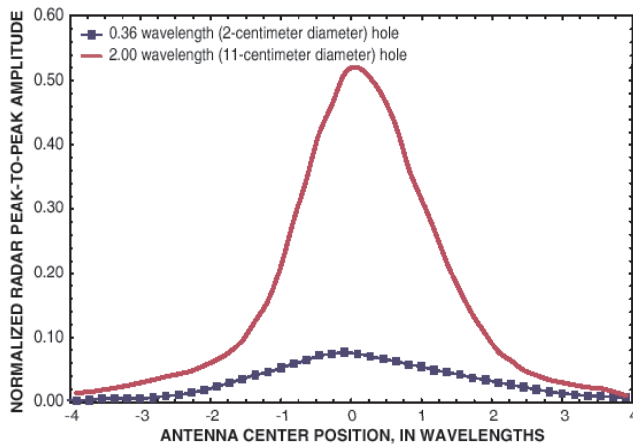


Figure 17. Normalized peak-to-peak amplitudes for waves transmitted in the physical model through the perfect-conductor analog for holes of 0.36 and 2.00 wavelengths (2 and 11 centimeters).

with the results of the 2D FDTD model.

The correlation between the amplitude trends predicted by the 2D FDTD numerical model and the amplitude trends observed in radar data acquired from the physical wall-edge and hole-in-wall models indicates that the numerical models can be used to interpret amplitude trends observed in cross-hole radar field data.

Electromagnetic Induction

EM-induction logs record the electrical conductivity or resistivity of materials or combinations of materials, such as the sediments and ground water, surrounding the borehole. EM-induction logging was conducted in every available borehole in the study area. The electrical conductivity of the formation was measured at 3.0-cm increments with a Mount Sopris 2PIA Poly Induction Probe. The probe has a vertical resolution of 40 cm and a radius of penetration of 100 cm (McNeill and others, 1990). EM-induction logs collected after iron injection were examined to deter-

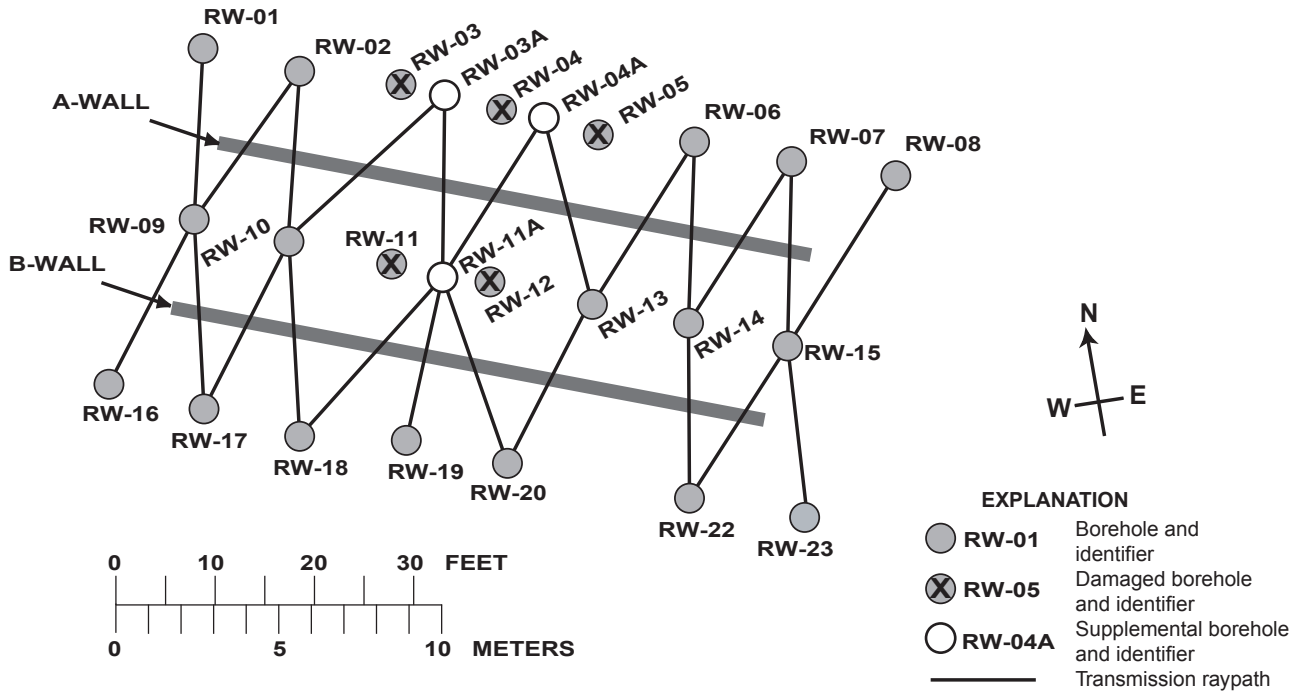


Figure 18. Map view of the study area showing observation boreholes and transmission raypaths, Massachusetts Military Reservation, Cape Cod, Mass. [Damaged boreholes were deformed during the iron-wall installation and were unusable for further radar data collection. The supplemental boreholes were drilled after the iron injection to replace the damaged boreholes.]

mine if the hydraulic-fracturing method resulted in the deposition of iron near the observation boreholes.

Processing of the EM-induction data included filtering and generating vertical sections using data from boreholes along the same row. The EM-induction logs were filtered with a 21-point moving-average filter to reduce random noise and the effects of small-scale spatial heterogeneities. EM-induction data from boreholes in the same row were combined into cross-section plots. EM-induction data collected in the northern row of boreholes (RW-01 to RW-07) after completion of the hydraulic fracturing are shown in figure 19. In this figure, an area with very high conductivity is present in boreholes RW-03, RW-03A, and RW-04A at a depth of about 28 m (fig. 18). These data indicate that highly conductive materials, interpreted as iron, were emplaced near these boreholes as a result of the injection process; and demonstrate, at least in this specific area, that the injection process resulted in a three-, rather than two-, dimensional distribution of iron.

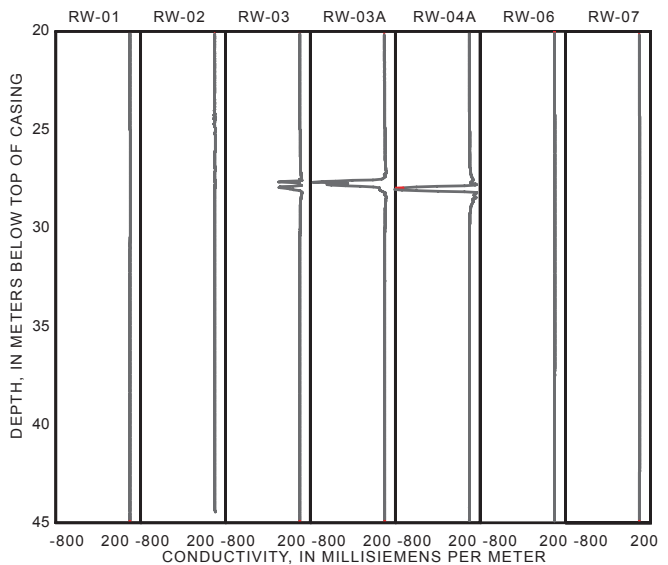


Figure 19. Borehole electromagnetic logging of boreholes north of the A-wall after the A-wall installation, Massachusetts Military Reservation, Cape Cod, Mass. [Negative values indicate the presence of highly conductive materials near the boreholes.]

Borehole Deviation

Borehole deviation logs record the three-dimensional (3D) geometry of a borehole. Borehole deviation logging was conducted to determine accurately the vertical orientation of the observation boreholes used for this study. This information is required to analyze the cross-hole radar data properly. Two independent borehole deviation surveys were conducted using a Century 9620 deviation and gamma probe and an Icefield Instruments, Inc. MI-03 series deviation tool. The Century tool was used to measure the deviation of boreholes RW-01 through RW-23 before the wall installation. The Icefield tool, which is dip based and unaffected by the presence of iron, was used after the iron injection to determine the geometry of boreholes RW-03A, RW-04A, and RW-11A.

Borehole deviation logs were combined with field-site survey information to produce 3D representations of the boreholes. These data were used to correctly position the locations of cross-hole radar traces. The borehole deviation data indicate that several boreholes deviate significantly from vertical.

Cross-Hole Radar Scanning

Cross-hole radar field data were acquired with a Malå GeoScience RAMAC borehole-radar system using electric-dipole antennas with center frequencies in air of about 100 and 250 MHz. Radar scans were conducted in 20 observation boreholes in three rows parallel to the injection zones (fig. 18). A radar scan of the region between two boreholes was constructed from cross-hole measurements acquired by moving a radar transmitter and receiver in unison at 10-cm increments from the top of the casing to the bottom of the borehole. At each antenna position, 32 traces were stacked (added) and recorded using a sampling frequency of 2,635 MHz and 1,024 samples per trace. The sampling rate was selected to ensure that frequency components within the radar-pulse frequency band were properly recorded.

Processing the cross-hole radar data was limited to band-pass filtering to reduce random noise. After filtering, the maximum peak-to-peak amplitude of the direct wave from each trace was measured (fig. 15). Under the assumption that iron was not introduced into sediments below a depth of 40 m, the amplitudes measured for each borehole-pair were nor-

malized relative to the average amplitude of “background” cross-hole measurements below 40-m depth. Thus, a normalized value near 1.00 indicates the pulse amplitude is consistent with a background value.

After normalization, amplitude data from each pair of rows were combined into cross sections and contoured. A contoured background cross-section image from the borehole pairs straddling the B-wall is shown in figure 20. Contoured post-injection cross-section images from borehole pairs straddling the A- and B-wall zones are shown in figures 21 and 22. In the post-injection plots of the A- and B-wall zones, strong amplitude decreases are observed in several areas of the cross-section coincident with the depths of iron injection (24 to 37 m).

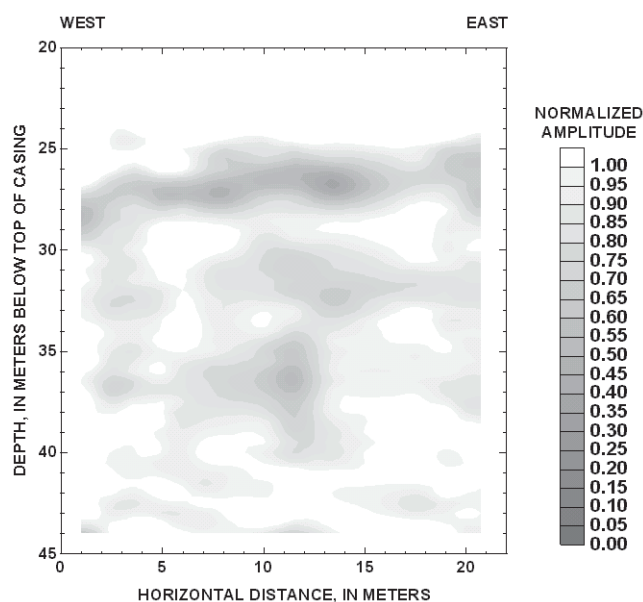


Figure 20. Pre-injection direct-wave amplitudes across the B-wall, Massachusetts Military Reservation, Cape Cod, Mass.

Before iron injection, it was assumed that the distribution of iron between borehole pairs would be identified by analyzing the differences in the normalized amplitudes between pre- and post-injection scans; however, because the hydraulic-fracturing process damaged five observation boreholes, the loss of these boreholes resulted in large data gaps (fig. 23) that prevented the use of a differencing approach. Therefore, normalized amplitudes from post-injection field-data were compared directly to the results of the numerical modeling.

Based on the numerical- and physical-modeling results, the following method was used to analyze

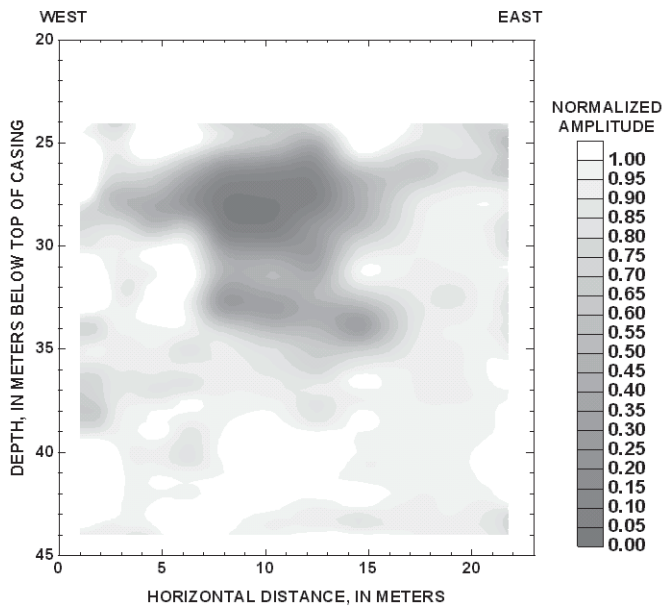


Figure 21. Post-injection direct-wave amplitudes across the A-wall, Massachusetts Military Reservation, Cape Cod, Mass.

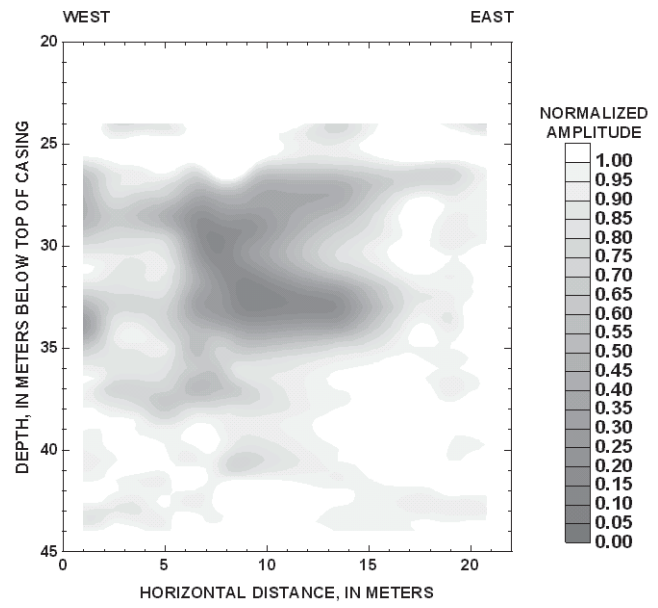


Figure 22. Post-injection direct-wave amplitudes across the B-wall, Massachusetts Military Reservation, Cape Cod, Mass.

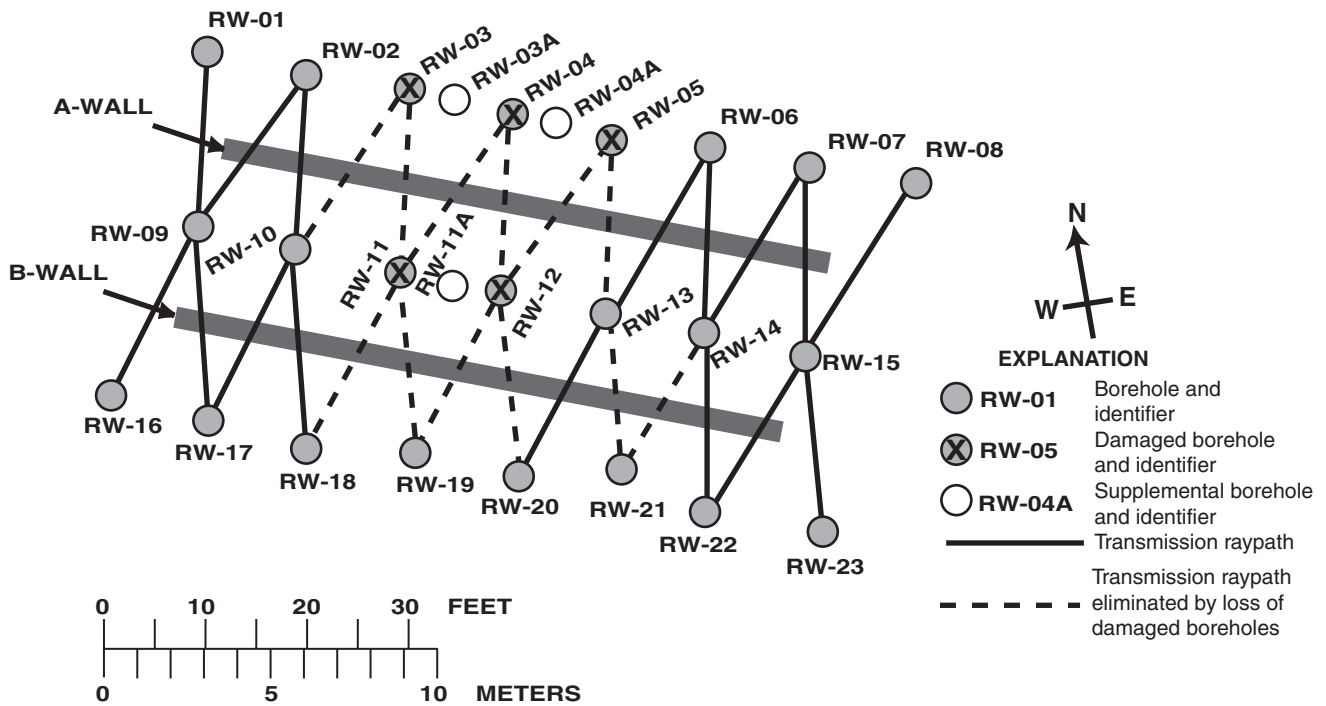


Figure 23. Map view of the study area showing observation boreholes and transmission raypaths lost due to damaged boreholes, Massachusetts Military Reservation, Cape Cod, Mass. [Damaged boreholes were deformed during the iron wall installation, and were unusable for radar data collection. The transmission raypaths from well pairs involving the damaged boreholes are shown with dashed lines. The supplemental boreholes were drilled after the iron injection to replace the damaged boreholes.]

the field data: (1) the depth where normalized post-injection amplitudes decreased to 0.43 was interpreted as a wall edge (fig. 8); (2) areas bounded by wall edges where amplitudes were below 0.43 were interpreted as wall zone; and (3) areas in a wall zone where normalized amplitudes exceeded 0.43 were interpreted as holes in a section of wall.

An example of this analysis applied to cross-hole radar data from the scan between boreholes RW-20 and RW-13 (fig. 18) is shown in figure 24. The field data are shown juxtaposed to the results of the numerical modeling. The vertical section of wall interpreted between boreholes RW-20 and RW-13 is about 3.10 m in height, extending from 31.7 m to 34.8 m below land surface. No holes are interpreted in this section of B-wall.

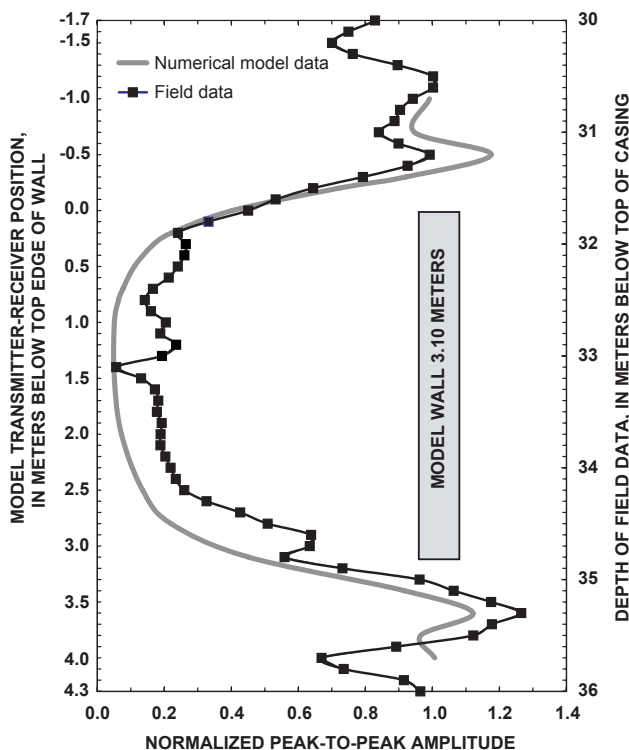


Figure 24. Normalized model-wall amplitudes for a 3.10-meter wall and the normalized field-data amplitudes from the common-depth radar survey between boreholes RW-20 and RW-13, Massachusetts Military Reservation, Cape Cod, Mass.

This analysis method was applied to the post-injection amplitude data from the A and B walls. Normalized cross-hole amplitude data below the 0.43 contour are shown for the A- and B-walls in figures 25 and 26. For the A-wall (fig. 25), the contouring outlines two irregularly shaped low-amplitude areas;

one extends about 10.0 m horizontally and 6.0 m vertically from about 25.0 to 31.0 m below land surface, and another zone extends about 8.0 m horizontally and 3.0 m vertically from about 31.5 to 34.5 m below land surface. For the B-wall (fig. 26), the contouring outlines a large irregularly shaped low-amplitude area that extends about 9.0 m horizontally and 7.5 m vertically from about 27 to 34.5 m below

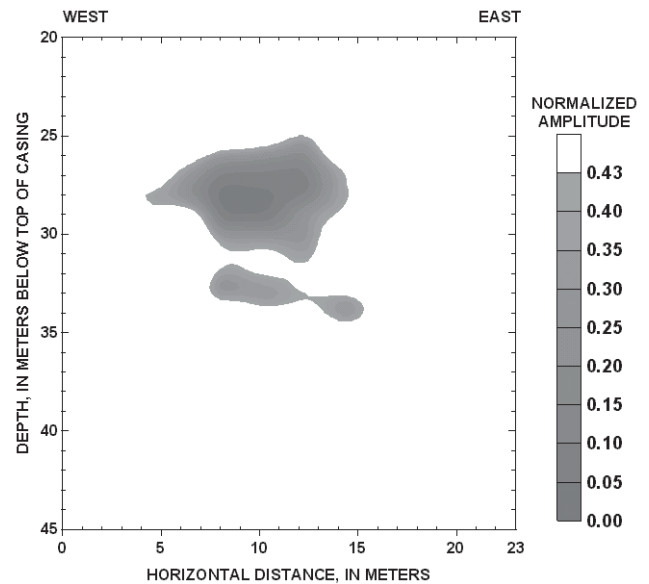


Figure 25. Post-injection direct-wave amplitudes across the A-wall showing normalized amplitudes of less than 0.43, Massachusetts Military Reservation, Cape Cod, Mass.

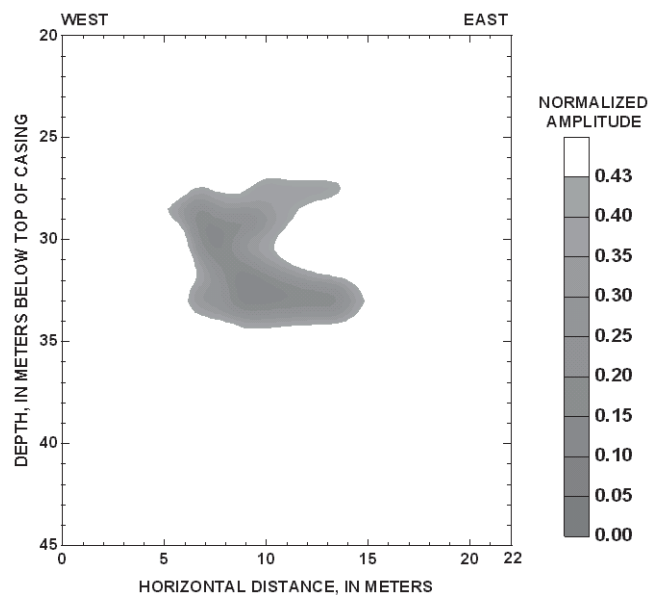


Figure 26. Post-injection direct-wave amplitudes across the B-wall showing normalized amplitudes of less than 0.43, Massachusetts Military Reservation, Cape Cod, Mass.

land surface. The continuous low-amplitude areas are interpreted as zones of iron wall.

Based on the numerical and physical modeling results, no observations in either the A- or B-walls indicated the presence of holes in the wall zones. This indicates that (1) iron in the wall zones is distributed in a generally continuous manner; (2) holes, if any, exist at scales smaller than the resolution limit of the radar antennas and acquisition geometry used for this study (about 10 cm); or (3) irregularities in iron distribution are such that holes in one area are masked by accumulations of iron in other areas.

SUMMARY

A pilot-scale study was conducted by the U.S. Army National Guard (USANG) at the Massachusetts Military Reservation (MMR) on Cape Cod, Massachusetts, to assess the use of a hydraulic-fracturing method to create vertical, permeable walls of zero-valent iron to passively remediate ground water contaminated by chlorinated solvents where the contamination is present at depths that exceed the practical construction limits of conventional iron walls. The study was conducted near the source area of the CS-10 plume, a chlorinated-solvents plume that underlies the MMR. In the study area, ground water is contaminated from about 24 to 37 m below land surface. A treatment zone consisting of two parallel, reactive-iron walls 12 m long, 0.15 m thick, extending from 24 to 37 m below land surface, and separated by about 6.1 m, was designed by the USANG to intersect and remediate a part of the CS-10 plume.

Because electrical conductors, such as iron, absorb electromagnetic energy, the U.S. Geological Survey used a cross-hole, common-depth, radar-scanning method to test the continuity and estimate the lateral and vertical extent of the two reactive-iron walls. The cross-hole radar surveys were conducted in boreholes on opposite sides of the iron injection zones using electric-dipole antennas with dominant center frequencies (in air) of 100 and 250 MHz. The amplitudes of radar waves crossing the injection zones decreased significantly between the pre- and post-injection surveys. Electromagnetic-induction data also showed significant changes between pre- and post-injection surveys of boreholes near the

injection zones.

Results from two-dimensional finite-difference time-domain numerical modeling and from laboratory-scale physical modeling were used to interpret the changes in radar amplitude observed in the field data. The numerical and physical models simulate a wall of perfectly conducting material embedded in saturated sand. Results from both the numerical and physical models indicate that the amplitude of a radar pulse transmitted across the edge of a conductive wall is about 43 percent of the amplitude of a radar pulse transmitted through background material. Simulation of radar pulse transmission through holes in perfectly conducting media indicates that holes with diameters less than about 40 percent of the wavelength of the dominant frequency of the radar pulse are not likely to be detected and that the amplitude of the transmitted radar pulse will increase as the diameter of the hole increases, approaching background levels as the hole aperture approaches the wavelength of the dominant frequency in the radar pulse.

Based on the results of the numerical and physical modeling, interpretation of the radar field data indicates that neither the A-wall nor the B-wall contain holes larger than about 10 cm, the resolution limit of the radar scanning in this study. However, the iron in the northern A-wall appears to be distributed in two discrete zones: an upper zone about 10-m wide, extending from about 25.0 to 31.0 m below land surface and a lower zone about 8-m wide, extending from about 31.5 to 34.5 m below land surface. The iron in the southern B-wall appears to be distributed continuously in a zone about 9-m wide extending from about 27.0 to 34.5 m below land surface.

The interpretation of the field data suggests that (1) the hydraulic-fracturing method introduced iron into the subsurface, but not in the dimensions originally proposed; (2) the iron within the treatment zones is distributed in a generally continuous manner; and (3) excluding the discontinuity in the A-wall, holes within the iron treatment zone, if any, exist at scales smaller than the resolution limit of the radar antennas and acquisition geometry used for this study. The cross-hole radar method appears to have been an effective method for delineating the distribution of iron in the two walls; however, the veracity of the results cannot be ascertained without excavation or drilling into the treatment zone.

REFERENCES CITED

- ABB Environmental Services, Inc., 1993, Task 2-5C remedial investigation field sampling and analysis plan, priority one areas of contamination: January 1993, various pagination.
- Carmichael, R.S., 1989, Practical handbook of physical properties of rocks and minerals: Boca Raton, Florida, CRC Press, Inc., p. 373.
- Gillham, R.W., and O'Hannesin, S.F., 1994, Enhanced degradation of halogenated aliphatics by zero-valent iron: *Ground Water*, v. 32, no. 6, p. 958-967.
- Hubble, D.W., and Gillham, R.W., 1997, Work plan for deep emplacement of granular iron PRW by vertical hydrofracturing and slurry injection - demonstration at CS-10 source area plume Massachusetts Military Reservation: Institute for Groundwater Research, Department of Earth Sciences, University of Waterloo, various pagination.
- Hubble, D.W., and Gillham, R.W., 1999, Installation of deep reactive walls at MMR using a granular iron-guar slurry, *in* Morganwalp, D.W., and Buxton, H.T., eds., U.S. Geological Survey Toxic Substances Hydrology Program-Proceedings of the Technical Meeting, Charleston, South Carolina, March 8-12, 1999: U.S. Geological Survey Water-Resources Investigations Report 99-4018C, v. 3, p. 431-438.
- Hubble, D.W., Gillham, R.W., and Cherry, J.A., 1997, Emplacement of zero-valent metal for remediation of deep contaminant plumes, *in* International Containment Technology Conference, St. Petersburg, Florida, February 9-12, 1997, Proceedings: Tallahassee, Florida, Florida State University, p. 872-878.
- Lane, J.W., Jr., Joesten, P.K., and Savoie, J.G., 1999, Monitoring a permeable reactive iron wall installation in unconsolidated sediments by using a cross-hole radar method, *in* Morganwalp, D.W., and Buxton, H.T., eds., U.S. Geological Survey Toxic Substances Hydrology Program-Proceedings of the Technical Meeting, Charleston, South Carolina, March 8-12, 1999: U.S. Geological Survey Water-Resources Investigations Report 99-4018C, v. 3, p. 439-445.
- McNeill, J.D., Bosnar, M., and Snelgrove, F.B., 1990, Resolution of an electromagnetic borehole conductivity logger for geotechnical and ground water applications: Geonics Limited, Technical Note TN-25, 28 p.
- Ricker, N., 1953, The form and laws of propagation of seismic wavelets: *Geophysics*, v. 18, p. 10-40.
- Savoie, Jennifer, and LeBlanc, D.R., 1998, Water-quality data and methods of analysis for samples collected near a plume of sewage-contaminated ground water, Ashumet Valley, Cape Cod, Massachusetts, 1993-1994: U.S. Geological Survey Water-Resources Investigations Report 97-4269, 208 p.
- Smyth, D.J.A., Shikaze, S.G., and Cherry, J.A., 1996, Hydraulic performance of permeable barriers for in situ treatment of contaminated groundwater, *in* Rumer, R.R., and Mitchell, J.K., eds., Assessment of barrier containment technologies, a comprehensive treatment for environmental remediation applications: Springfield, Virginia, National Technical Information Service, p. 881-886.
- Starr, R.C., and Cherry, J.A., 1994, In situ remediation of contaminated ground water--the funnel-and-gate system: *Ground Water*, v. 32, no. 3, p. 465-476.
- Xiao, Lei; Liu, Lanbo; and Cormier, V.F., 1998, Two-dimensional finite-difference time-domain solution for Maxwell's equations using pseudo-spectral method, *in* Seventh International Conference on Ground Penetrating Radar (GPR'98), Lawrence, Kansas, May 27-30, 1998, Proceedings: Lawrence, Kansas, Radar Systems and Remote Sensing Laboratory, p. 585-589.

Lane and others, 2001--Cross-Hole Radar Scanning of Two Vertical, Permeable, Reactive-Iron Walls at the Massachusetts Military Reservation, Cape Cod, Massachusetts
U.S. Geological Survey Water Resources Investigations Report 00-4145